Investigation of tolerance for icing of UAV rotors/propellers: phase 3 test rig development and calibration

Orchard, D. M.

Laboratory Technical Report (National Research Council of Canada. Aerospace. Aerodynamics Laboratory); no. LTR-AL-2021-0045, 1, 2021-08-12

NRC·CNRC

AERODYNAMICS LABORATORY

Investigation of Tolerance for Icing of UAV Rotors / Propellers - Phase 3 Test Rig Development and Calibration

Unclassified

Limited

LTR-AL-2021-0045

12/08/2021

Dr. D.M. Orchard

National Research Council Canada
Conseil national de recherches Canada

Canada

AERODYNAMICS LABORATORY

Investigation of Tolerance for Icing of UAV Rotors / Propellers - Phase 3 Test Rig Development and Calibration

Volume 1

Report No.: LTR-AL-2021-0045

Date: 12/08/2021

Authors: Dr. D. M. Orchard

Classification :	Unclassified **Distribution:** Limited
For:	Transport Canada – RPAS Task Force Engineering
SIGMA ID#:	A1-018255
Submitted by:	Dr. Michael Benner, **Director R & D, Aerodynamics Laboratory**
Approved by:	Dr. Mouhab Meshreki, **Director General (Acting), Aerospace Research Centre**

Pages :	32	**Copy No :**	1
Figures :	36	**Tables :**	3

ABSTRACT

This report details the development and calibration of a new facility to test medium size rotors for Remotely Piloted Aerial Systems (RPAS) under in-flight icing conditions. This facility has made use of a 3 m x 6 m cold room at the Montreal Road campus of the NRC and includes a spray bar system to provide the icing cloud as well as a dedicated rotor stand assembly that incorporates a load cell and dynamometer. Calibration data of the spray drop sizes and liquid water content are provided and compared to conditions of the natural environment as detailed in icing regulations for transport category airplanes, i.e., CFR 14 Part 25 Appendix C and O. Example data of performance of a medium size rotor under icing conditions are provided and compared to previous data collected on smaller rotors in a different icing facility at the NRC.

NOMENCLATURE

AEDC	Arnold Engineering Development Centre
AIWT	Altitude Icing Wind Tunnel
CM	Continuous Maximum
Dmax	Maximum Droplet Diameter
ESC	Electronic Speed Controller
g	Gravity, m/s^2
IM	Intermittent Maximum
LWC	Liquid Water Content, g/m^3
$\dot{m}$	Mass Flow Rate, kg/s
MVD	Median Volumetric Diameter, μm
P_{air}	Spray Air Pressure, Pa
r	Drop Radius, m
RPAS	Remotely Piloted Aerial System
RPM	Revolutions per Minute
SLD	Supercooled Large Drop
UAS	Unmanned Air System
UAV	Unmanned Air Vehicle
V_t	Terminal Velocity, m/s
WFR	Water Flow Rate, L/min
ZLE	Freezing Drizzle
ZRE	Freezing Rain
ρ	Density of air, kg/m^3
ρ_w	Density of water, kg/m^3

Table of Contents

Contents

1 Introduction

Aircraft encounters with icing conditions during flight are recognized as a major safety hazard, with the accretion of ice on critical surfaces leading to degradation of aerodynamic performance, such as increasing drag, degrading control authority and decreasing the ability of an airfoil to lift along with stall occurring at much higher speeds and lower angles of attack than normal [1] The threat posed by in-flight icing encounters is particularly concerning for Unmanned Air Systems (UAS's) that operate at lower altitudes and lower speeds, where the frequency of icing events is increased and the resulting ice accretion enhanced compared to larger aircraft. In addition, UAS's often lack the ability to detect the occurrence of an icing event from which the risk can be assessed and appropriate corrective action performed.

When a UAS encounters icing conditions, a particular concern is the degradation in the performance of the rotors and propellers. The blades tend to collect ice rapidly, leading to loss of thrust, abrupt increase of power consumption and, with sufficient exposure to the icing environment, catastrophic failure of the vehicle. To address this, over the last two years the NRC and Transport Canada (TC) have entered into collaborative research agreements as part of TC's Remotely Piloted Aerial Systems (RPAS) task force with the objective of creating an evidence-based regulatory framework for safe UAS operations in Canadian airspace. Phase 1 of this work [1] (FY 18/19) provided an extensive literature review and the acquisition and development of equipment for the simulation of propeller icing within a wind tunnel environment. Phase 2 of this work [3] (FY 19/20) continued with tests performed on small propellers (i.e., between 10" to 14" diameter) under a range of icing conditions in the NRC Altitude Icing Wind Tunnel (AIWT). This study demonstrated the influence of various icing parameters, such as drop size (median volumetric diameter, MVD), temperature and liquid water content (LWC), on reducing thrust and increasing power input requirements of UAS propellers.

This project represents Phase 3 of the study assessing the icing risks to RPAS and extends the work of Phase 2 by testing larger diameter rotors. This phase of the project places emphasis on the development of a test cell that can provide a realistic simulation of the type of icing conditions an RPAS will encounter in the Canadian environment, i.e., freezing drizzle and freezing rain.

2 Objectives

The data provided by the Phase 2 RPAS icing study [3] was obtained using small propellers within an icing wind tunnel, namely the NRC AIWT. This work provided important insight into the degradation of aerodynamic performance of propellers subjected to in-flight icing conditions. The test conditions used in the Phase 2 study were chosen to represent standard icing environments for civil aviation platforms for flight through clouds containing supercooled water droplets. Although this is not a full representation of the icing conditions that an RPAS may encounter during operation, i.e., altitude < 400 ft and below the cloud base, the wind tunnel was chosen as it has a calibrated icing environment (e.g., MVD, LWC, etc.) and aerodynamic environment (e.g., velocity, static temperature, etc.).

The objective of Phase 3 is to extend this work by examining the aerodynamic performance of larger propeller diameters under icing. However, due to size constraints of the AIWT test section, an alternative (larger) test facility capable of providing a simulated icing environment was required. While, a preliminary review highlighted a number of potential test facilities that could accommodate this work, these facilities did not offer the necessary precision and accuracy in terms of simulating the icing conditions expected to be found in nature.

With this in mind, it was proposed that Phase 3 be divided into two main objectives:

- Development of an RPAS icing facility in the NRC M17 cold room
- Use of the RPAS icing facility to assess performance under icing of larger (>20" diameter) propellers

Developing a unique and dedicated RPAS icing facility allows the cloud conditions to be carefully controlled and calibrated to provide close representation of natural atmospheric conditions. Following the initial development, the facility will provide a fully calibrated, low cost and accessible test capability necessary for the testing of larger diameter RPAS rotors. As well as accommodating the test requirements of Phase 3, it is envisaged that the test facility will provide a longer-term solution for assessment of RPAS concepts under icing conditions.

3 The RPAS Icing Environment

Until recently, the icing envelopes used for the certification of transport category airplanes have been in accordance with the Title 14 Code of Federal Regulations (CFR) Part 25 Appendix C [4]. However, following the accident of an ATR-72 at Roselawn, Indiana in 1994, the National Transport Safety Board report [5] concluded that the 14 CFR Part 25 Appendix C icing envelope has limitations regarding certification in conditions that contain supercooled large droplets (SLDs) with diameters in excess of 100 μm.

Therefore, when evaluating the flight environment for the assessment of propeller performance in icing conditions, a combination of different conditions that encompass Appendix C, freezing drizzle and freezing rain encounters (as defined by Appendix O of CFR 14 Part 25 [6]) all need to be considered. Details of these conditions are given below.

3.1 Appendix C Icing

Appendix C icing conditions fall into two categories that describe the relationship between MVD, static air temperature and LWC. These are referred to as Continuous Maximum (CM), which has lower LWC but longer horizontal extent of the cloud and a maximum MVD of 40 μm, and Intermittent Maximum (IM), which generally has higher LWC over shorter distances and a maximum MVD of 50 μm. For the purposes of the current RPAS icing considerations of this project, which limits potential operation to a maximum of 400ft, as IM icing does not occur below 4000 ft, only CM icing is considered as part of the potential flight envelope. The relationship between drop size, LWC and temperature for Appendix C CM icing is shown in Figure 1.

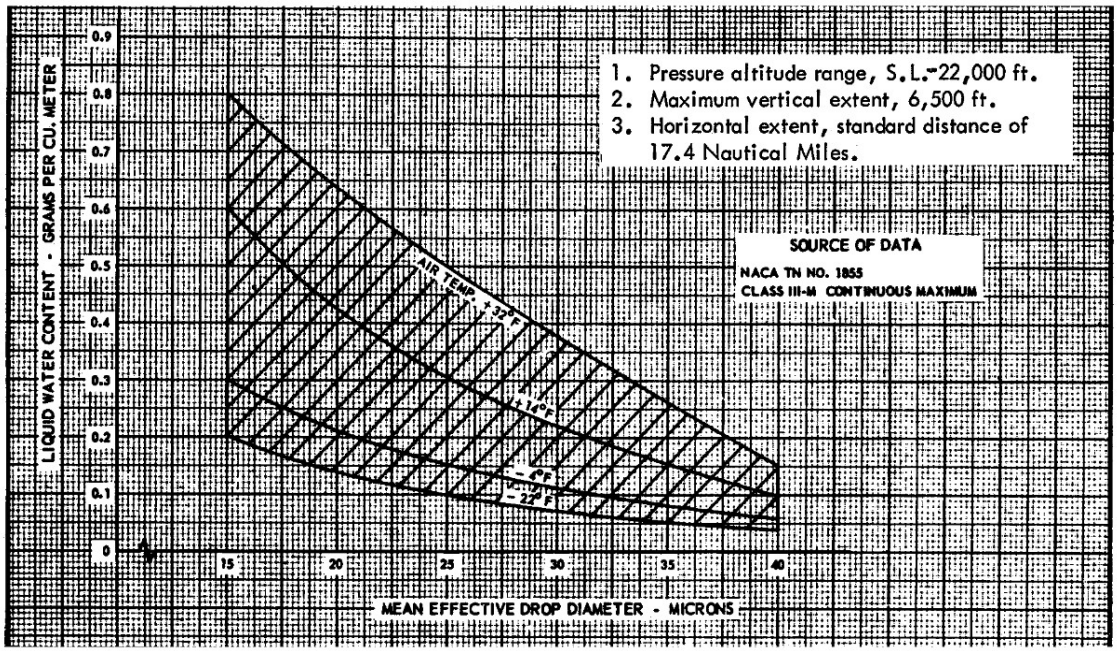

Figure 1: Continuous Maximum Icing Envelope [4]

3.2 Freezing Drizzle and Freezing Rain

Supercooled Large Drop icing can be effectively represented as either freezing drizzle, for which the maximum droplet diameter, Dmax, is less than 500 µm (denoted by the abbreviation ZLE), or freezing rain, for which Dmax is greater than 500 µm (denoted by the abbreviation ZRE). The data is then further segregated into states where the MVD is less or more than 40 µm (Cober et al. [7], Cober and Isaac [8]). These four distinct SLD environments are characterized in terms of MVD and Dmax, as shown in Table 1

In addition to the larger drop sizes, SLD differs from Appendix C icing by displaying a bi-modal nature across the particle mass distributions. The extent of the bi-modality differs across the four distinct categories as shown in the cumulative mass distributions and normalized mass distributions given in Figure 2 and Figure 3 respectively.

Table 1: Segregation of SLD conditions

Definition	Abbreviation	MVD (µm)	Dmax (µm)
Freezing Drizzle	ZLE_in	20	389
	ZLE_out	110	474
Freezing Rain	ZRE_in	19	1553
	ZRE_out	526	2229

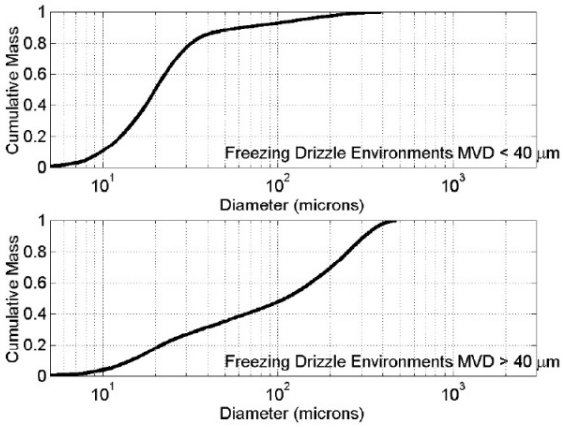

a) Drop cumulative mass distributions for freezing drizzle

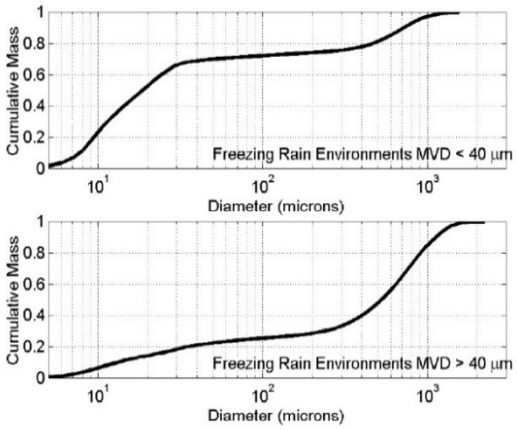

b) Drop cumulative mass distributions for freezing rain

Figure 2: Drop cumulative mass distributions for SLD environments

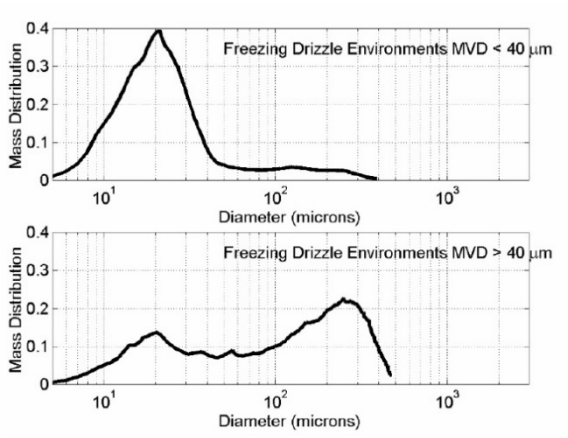

a) Normalized mass distributions for freezing drizzle

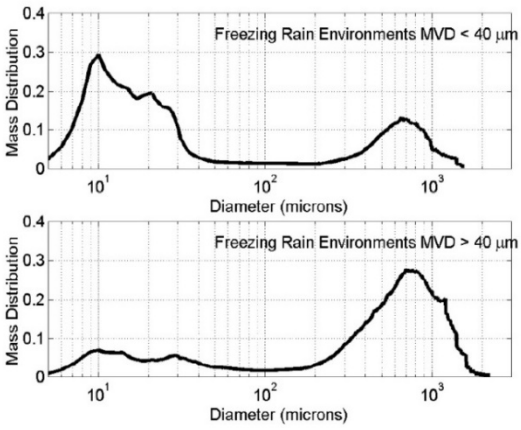

b) Normalized mass distributions for freezing rain

Figure 3: Normalised mass distributions for SLD environments

In addition to representing a spray profile in terms of MVD and particle distribution, a simulation of the SLD environment needs to achieve these conditions with consideration for the representative LWC's and static temperatures. These are shown in Figure 4 indicating freezing drizzle icing conditions can be expected down to as low as -25° C with LWC's ranging from 0.18 g/m^3 at -25°C to 0.44 g/m^3 at 0°C.

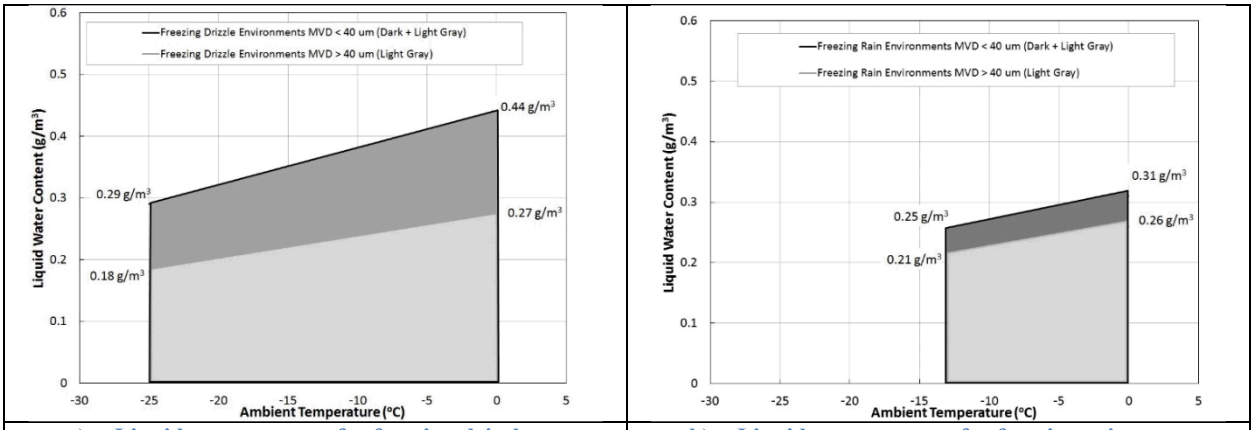

a) Liquid water content for freezing drizzle

b) Liquid water content for freezing rain

Figure 4: Liquid water content for SLD

4 Development of the RPAS Icing Test Facility

In order to extend the work of Phase 2 tests by using larger diameter rotors, an alternative (larger) test facility capable of providing a simulated icing environment was required. As previously mentioned, existing facilities did not offer the necessary precision and accuracy in terms of simulating the icing conditions expected to be found in nature. It was therefore decided to make use of a 3 m x 6 m cold room located at the NRC Montreal Road campus (building M17) and develop a calibrated spray system in this facility. In doing this, the icing conditions could be specifically calibrated to the needs of this project and would result in a readily available icing test facility for this and any follow on projects. The only limitation of the cold room is that it cannot provide any wind which would simulate the forward speed of a propeller, or the climb of a rotor.

The concept of the cold room icing rig is shown in Figure 5 and includes a mounting stand for the propeller assembly on the floor and a series of air-atomizing spray nozzles mounted from the ceiling to provide the icing cloud. The rotor mounting system comprises a motor, load cell and dynamometer, and is mounted 1.8 m beneath the spray system. The distance between the nozzle system and the test article is an important parameter when considering the simulation of icing clouds in test facilities as the water drops require adequate residence time to attain equilibrium temperature with the surrounding airflow. To determine the necessary distance required to attain drop supercooling, the Arnold Engineering Development Center 1 Dimensional Multiphase (AEDC 1DMP) code [9][10] was used that provides calculation of the drop conditions throughout the travel from injection into the test environment to the test article. It should be noted, however, that the drop temperature calculation was performed assuming terminal velocity of the water drops without the influence of increased speed due to the thrust of the rotors and further analysis is required to examine the influence of the flow field on the drop properties. The control and data acquisition of all systems (rotor speed, thrust measurement, spray control etc.) is performed via dedicated hardware located outside of the cold room.

The spray system has a target range of icing cloud conditions with MVDs between 50 µm to 500 µm and with LWC up to 1 g/m^3, thus enabling testing across a range of conditions from typical civil aviation icing environments (e.g., Appendix C of 14 CFR Part 25) up to those experienced in freezing drizzle precipitation. Before the spray system was installed in the cold room, a series of tests were performed in order to calibrate the environment in terms of drop size distribution and LWC of the cloud.

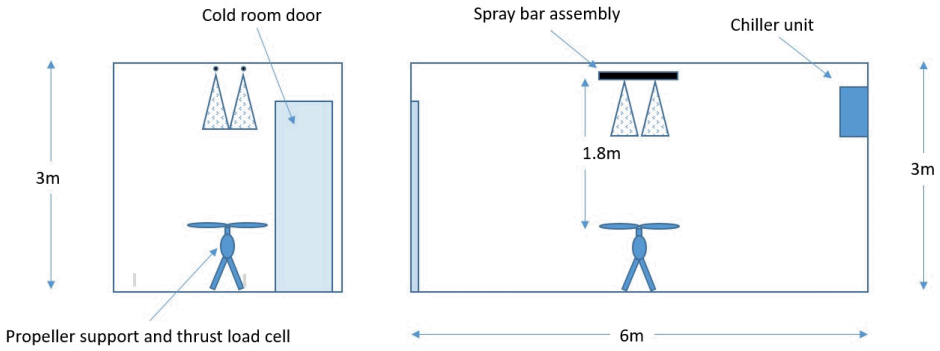

Figure 5: Concept of RPAS Icing Facility

4.1 Spray Rig

The spray rig includes four externally mixed, air atomizing nozzles connected to metered water and pressurised air supplies. A schematic of the spray system is shown in Figure 6. The water supply is provided by a pump connected to a tank of distilled water. Flow is controlled using an Alicat LC 200CCM-D flow controller connected to the main computer Data Acquisition (DAQ) system that enables the bulk water supply to be adjusted up to 200 cm^3/min. Downstream of the flow controller the water is split into four individual supply lines and passed through float element flow valves that allow the water supply to each of the four nozzles to be balanced. The flow lines are then fed to solenoids that direct water flow to the nozzles (spray on condition) or back to the supply tank (spray off condition). While the solenoids are placed outside of the cold room to avoid issues with the water lines freezing, they are as close as possible to the nozzles inside the cold room to keep the length of the water supply lines to a minimum and reduce the time between spray activation and spray onset.

Pressurised air is provided by the main 'shop' air supply of the building and is split into three separate lines to provide control of the air-actuated solenoid, purge air to the water supply lines and atomizing air to the nozzles. The atomizing air flow is controlled via a hand-operated regulator and the pressure measured by a transducer with the output provided to the DAQ system. The purge air is attached to the spray control solenoid and, when the system is in the spray off condition, the air is fed through the nozzle water supply line to remove any standing water in the line to prevent it from freezing.

A thorough calibration of the air supply pressure and water flow rate to provide the required MVDs and LWCs was required as part of the system commissioning process. This process is described in the next section.

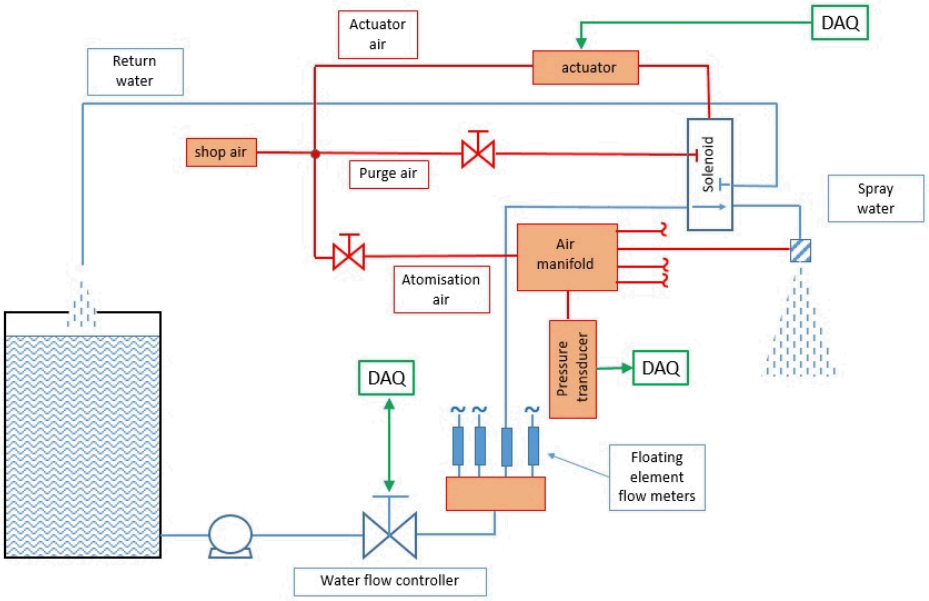

Figure 6: Schematic of the RPAS icing facility spray system

5 Spray System Calibration

The main calibration was performed outside of the cold room with the spray system installed on a frame as shown in Figure 7. This frame consisted of an array of four nozzles mounted 1.8 m above a grid of 25 test tubes used to capture water over an area of 0.23 m^2 (360 in^2). The nozzles were mounted to the frame to allow their relative spacing to be adjusted for optimization of the water distribution at the measurement location below, as shown in Figure 8.

Figure 7: Spray system calibration rig

Figure 8: Nozzles installed on spray system calibration rig

5.1 Water Content Calibration

As previously mentioned, an array of 25 test tubes were installed beneath the spray nozzles to capture water during the spray on process. By measuring the overall water captured by the tests tubes, it was possible to determine the distribution of the water spray at the measurement locations, calculate the average 'rainfall'

rate (in Litres/hour/m^2) and thereby calibrate the system to an appropriate simulation of the natural environment.

The tubes were installed in a rectangular frame (see Figure 9) and spaced 0.127 m (5”) from left to right and 0.114 m (4.5”) from top to bottom and, to increase the capture area, a 0.0254 m (1”) diameter funnel was placed into the opening of each tube. A view of this arrangement showing the test tubes with funnels installed in the test frame is shown in Figure 10.

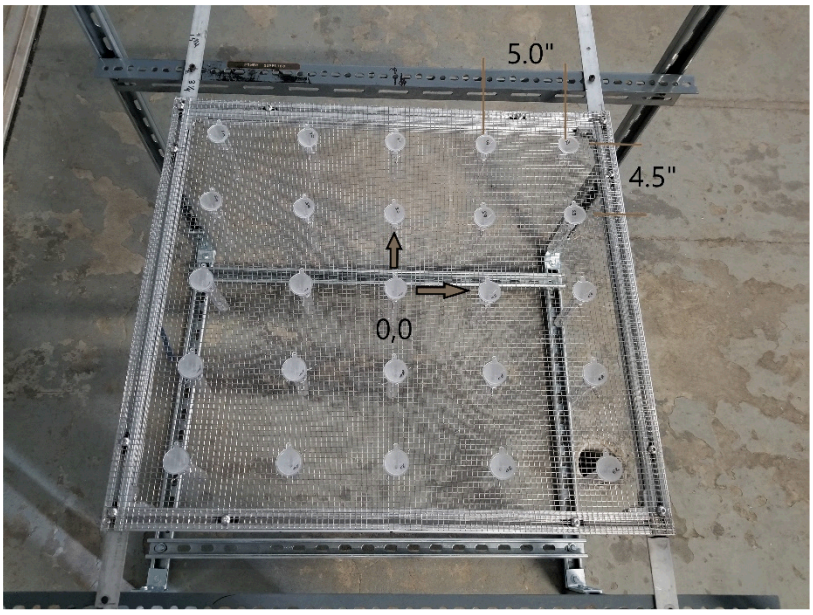

Figure 9: Water capture tubes installed in the calibration rig

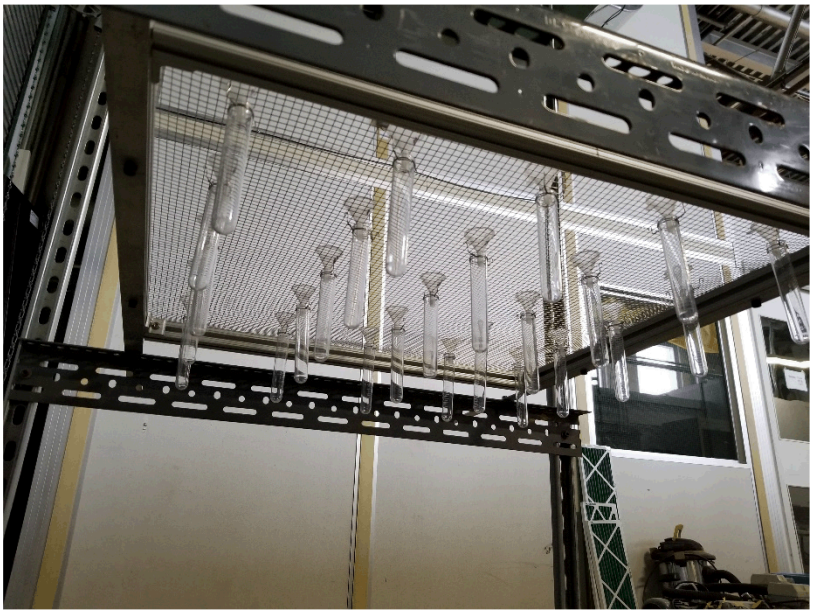

Figure 10: Water capture test tubes (with funnels) suspended from the rectangular frame installed on calibration rig

To measure the water distribution, the spray system was operated at a pre-set water flow rate, *WFR*, air

pressure, P_{air}, and time, *t,* following which the water collected in each tube was weighed to provide a local measurement of water flow rate in L/hr. The local water flow measurements were then averaged over the measurement area to provide a measurement of rainfall in L/hr/m^2.

Prior to performing the calibration, the optimal spacing of the nozzles was determined through a series of tests using 4 different configurations, specified here as A to D. The water flow distributions obtained from the four configurations are shown in Figure 11 to Figure 14 and indicate that spray nozzle configurations A and B were too close together resulting in a peak of water distribution in the center of the measurement area. Configuration D suggests that the nozzles were too far apart, resulting in areas of reduced water flow in the centre. The nozzle configuration C demonstrated the most even water spray distribution and this setting was used for all subsequent calibrations.

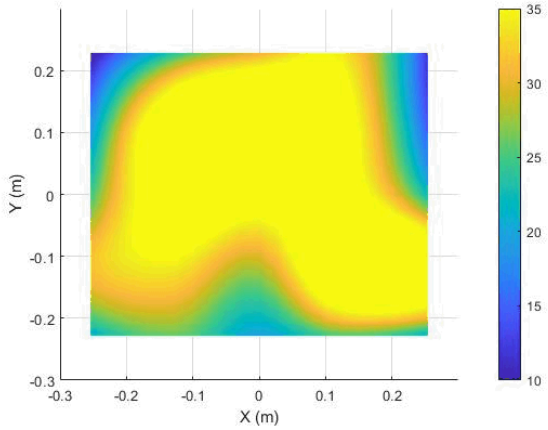

Figure 11: Water capture distribution with nozzles in configuration A (L/hr/m^2)

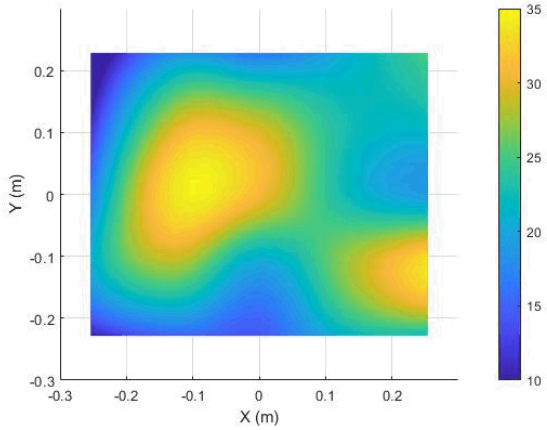

Figure 12: Water capture distribution with nozzles in configuration B (L/hr/m^2)

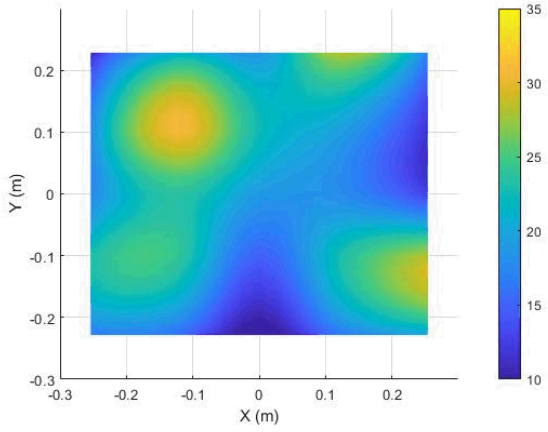

Figure 13: Water capture distribution with nozzles in configuration C (L/hr/m^2)

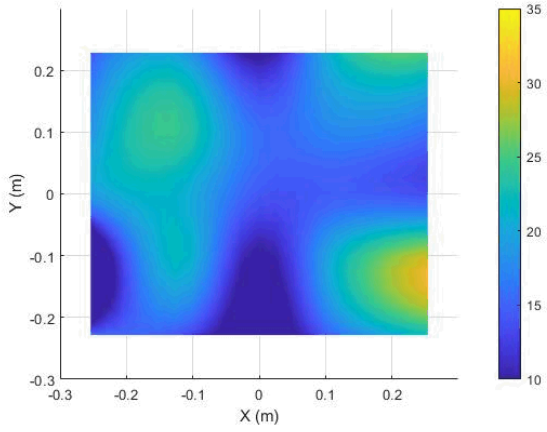

Figure 14: Water capture distribution with nozzles in configuration D (L/hr/m^2)

Once the nozzle configuration was determined, a series of tests were performed at four different water flow rates (i.e., 25 cm^3/min, 50 cm^3/min, 100 cm^3/min and 150 cm^3/min) and the corresponding rainfall rates calculated, as shown in Figure 15. On this graph, three distinct rainfall regions are also identified as light, moderate and heavy and show that the spray system is capable of achieving rainfall simulation consistent

with natural precipitation across all three conditions.

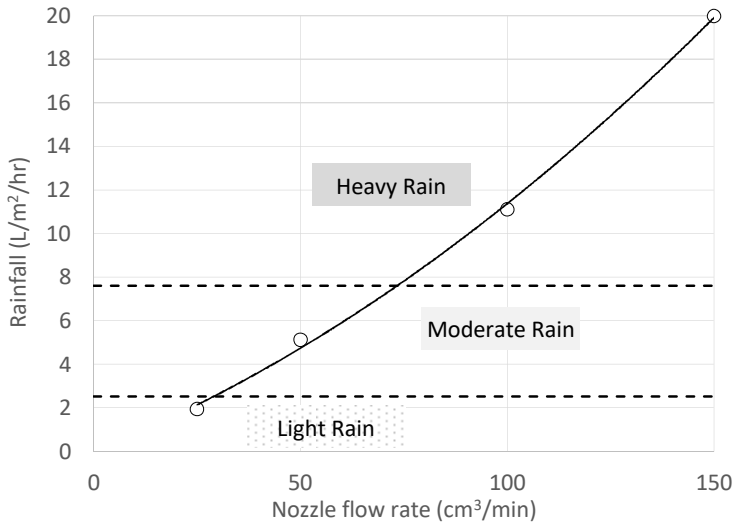

Figure 15: Rainfall rate v nozzle water flow rate

While the spray conditions have been given in terms of rainfall rate, it is also necessary to relate this to LWC in g/m^3 to be consistent with the nomenclature of in-flight icing regulations such as Appendix C and O. However, as LWC is a function of airspeed, the terminal velocity, V_t, of a drop must be used in this calculation where V_t is defined as,

$$V_t = \sqrt{\frac{8\, r\, \rho_w\, g}{3\, \rho\, C_D}}$$

Where r is the radius of the drop, ρ the density of air, ρ_w the density of water, g acceleration due to gravity and C_D the drag coefficient for a sphere (= 0.5 for these Reynolds numbers). Once V_t is known the LWC can be calculated from,

$$LWC = \frac{\dot{m}}{Area\,.V_t}$$

Where $\dot{m}$ is the mass flow provided by the rainfall measurements. Consequently, as V_t increases with drop size, for the same rainfall rate, the LWC will reduce. This is demonstrated in Figure 16 showing the LWC's compared to nozzle flow rate over a range of drop MVD's from 60 µm to 300 µm.

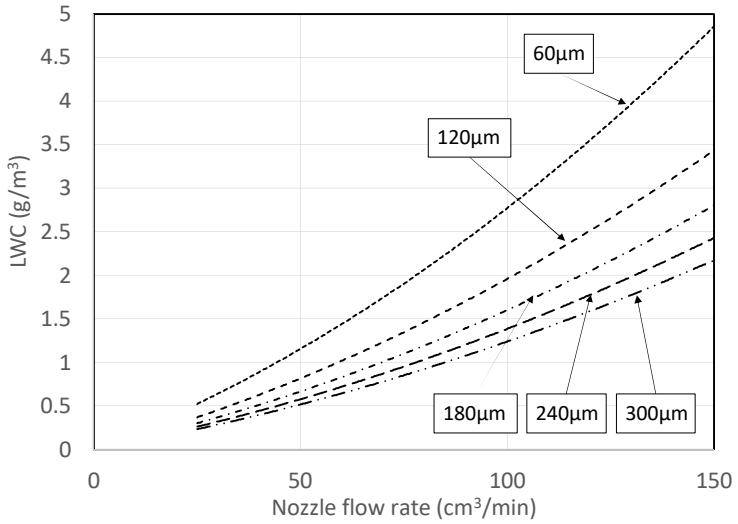

Figure 16: LWC's with water flow rate as a function of drop size

5.2 Drop Size Calibration

A Malvern Spraytec particle size analyzer was used to measure the drop size spectrum of the spray system. This system has the ability to measure drop sizes from less than 10 µm up to 2.5 mm and was mounted on the floor adjacent to the spray rig as shown in Figure 17.

The drop sizes measured over a range of atomizing air pressures from 0.5 psi to 5.5 psi are shown in Figure 18 and give MVDs ranging from 350 µm to 60 µm respectively. During these measurements, the water flow rate was also varied at each air pressure (i.e., 12 cm^3/min, 25 cm^3/min and 50 cm^3/min).This was not shown to affect the drop size calibration, with the MVD being solely a function of atomizing air pressure.

From these measurements, a power law fit of MVD verses atomizing air pressure was applied to the data to obtain a calibration curve for inclusion in the data acquisition and control system. This curve is shown in Figure 18 and the comparison of this to the measured data given in Figure 19. As shown, across the full range of drop sizes, all measured MVD's are within ±20% of the calibration, however this difference drops to ±10% of the calibration for all drop sizes less than 300 µm.

Particle spectrum distributions taken from the Malvern measurements for MVDs of 60, 120, 200 and 300 µm are shown in Figure 20, Figure 21, Figure 22 and Figure 23 respectively. Apart from the 300 µm MVD case, all distributions display a bi-modality to the spray profile with a main distribution centered on the MVD value with a second 'hump' above 1 mm drop diameter drop. This secondary profile is considered to be a result of smaller drops coalescing as they drop from the spray nozzles.

Figure 17: Malvern Spraytec mounted adjacent to the spray calibration rig

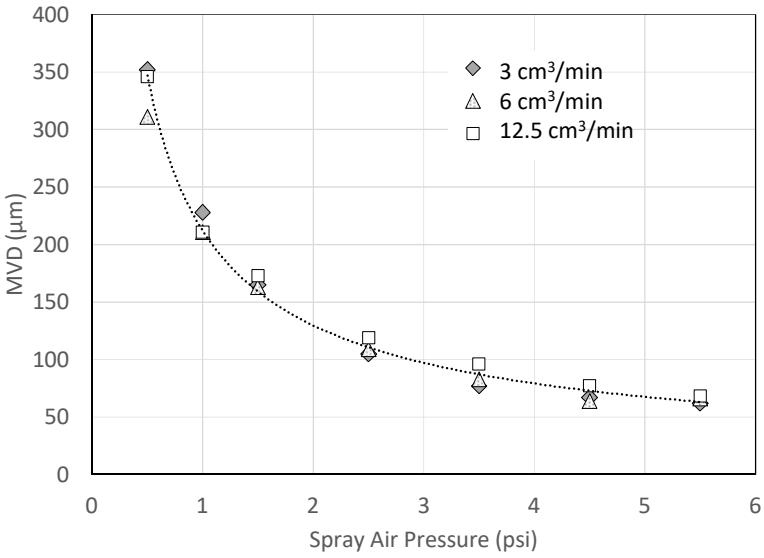

Figure 18: Measured drop size distribution with spray air pressure

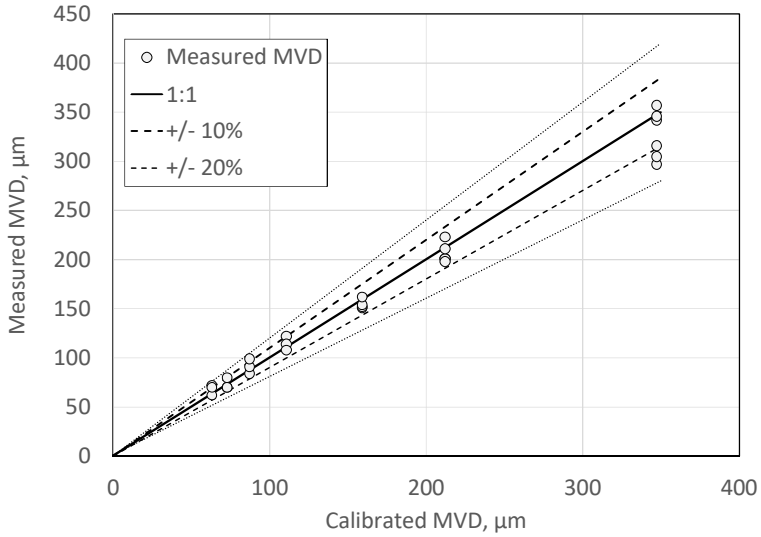

Figure 19: Comparison of measured drop size to calibration

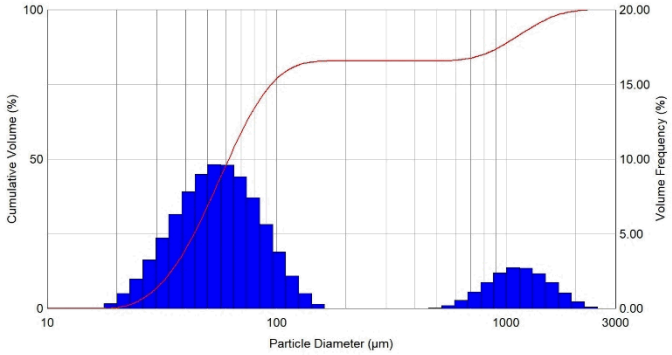

Figure 20: Drop size distribution for MVD = 60 µm

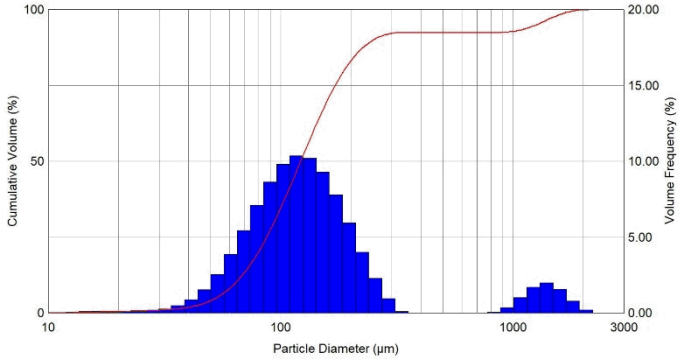

Figure 21: Drop size distribution for MVD = 120 µm

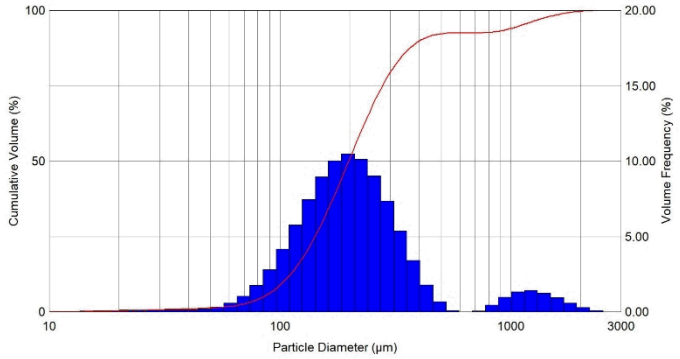

Figure 22: Drop size distribution for MVD = 200 µm

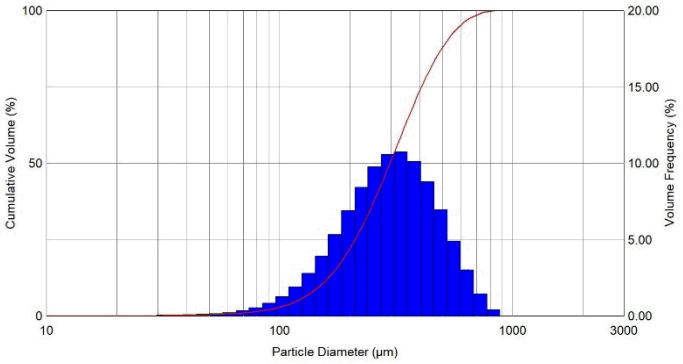

Figure 23: Drop size distribution for MVD = 300 µm

5.3 Comparison to RPAS Flight Environment

For the purposes of the current study, the test rig performance is evaluated against environmental conditions expected for flight of RPAS for which the maximum altitude is not expected to exceed 400 ft. Therefore, in-flight icing conditions defined by Appendix C (CM) and Appendix O (freezing drizzle and rain) are considered. In addition, with the low altitude of the RPAS flight envelope, consideration would also need to be given to ground icing encounters such as freezing precipitation.

While the LWC capability of the test rig has been shown to lie within a range expected for Appendix C conditions, the minimum MVD included in the calibration procedure (i.e., 60 µm) is higher than the maximum value for this icing envelope. Therefore, for the current study, simulation of Appendix C is performed at higher drop sizes than those specified by this regulation and future work is required to extend the icing test rig calibration to lower MVD's.

For Appendix O, the calibration has shown the MVD is controllable from 60 µm to 350 µm and therefore capable of achieving drop sizes consistent with the requirement of freezing drizzle with MVD > 40 µm. Limiting the MVD to a minimum of 60 µm, however, has meant that freezing drizzle and freezing rain conditions with MVD < 40 µm cannot be fully matched in terms of drop size mass distribution and further calibration effort is required to capture these points. As a result, for the current work, simulation of these conditions is performed at higher MVD's than specified in the regulation. For freezing rain with MVD > 40 µm, the current calibration extends to drop sizes less than the MVD specified for this condition (i.e., 526 µm) and simulation is limited to the maximum MVD's measured in the current data set (i.e., 350 µm).

Despite the current limitations in matching the MVD's to icing regulations, the calibration has shown a

wide range of drop size settings are available, enabling the sensitivity of RPAS rotors to MVD to be evaluated. In addition, as a result of drop coalescing, the particle size distributions have shown the profiles display a natural bi-modality which lends itself to matching this aspect of Appendix O icing conditions.

Measurements have shown a wide range of LWC's (from 0.2 g/m^3 to greater than 5 g/m^3) are achievable with this test rig, thus enabling simulation of water content conditions characteristic of those expected for Appendix O SLD as well as for heavy precipitation conditions.

6 Rotor Thrust Stand

The test rig consists of an RC Benchmark (Tyto Robotics Inc.) Series1780 Dynamometer 25kgf-100A: Single-motor, a XOAR Titan T8110 140KV brushless electric motor and a Xoar Pulse P80 electronic speed controller (ESC). The RC Benchmark Series 1780 Dynamometer is shown in Figure 24 and its design specifications are provided in Table 2. The dynamometer is equipped with load cells and accelerometers to directly measure torque, thrust and accelerations due to vibrations, respectively. It also provides direct measurements of voltage, current, RPM, and motor winding resistance.

Table 2: RCBenchmark Series 1780 thrust stand details

Specification	Min	Max	Tolerance	Unit
Thrust	-25	25	±0.5%	kgf
Torque	-12	12	±0.5%	Nm
Voltage	0	60	±0.5%	V
Current	0	100	±1%	A
Angular speed	0	190		k-RPM

Figure 24: RC Benchmark thrust stand example

For the current set up, as the rotor blade was to be installed in the horizontal plane, a slight modification to the thrust stand set up was required whereby the load cell and motor were rotated 90^o. Also, as the full assembly would be exposed to the cloud, a housing was manufactured that protected the electrical

components from the wet environment. The motor full assembly (with the rotor blade rotated 90°) with the protective housing is shown in Figure 25.

Figure 25: Thrust stand assembly with protective housing

7 Rotor Blade

As one aim of this project was to extend the work performed in Phase 2 on small diameter rotor blades to larger diameter test articles, a 22" diameter carbon fibre Mejzlik (7.4° pitch) propeller was chosen as the test article for this study as shown in Figure 26 . Tests were also performed with a 12" diameter carbon fibre (6° pitch) blade to provide a comparison to data obtained during the Phase 2 tests within the AIWT.

Figure 26: Test rotor blade – Mejzlik 22" diameter 7.4° pitch

8 Cold Room

Following the calibration process, the spray system and rotor assembly were installed in the 3 m x 6 m cold room located in building M17 of the NRC Montreal Road campus. The temperature in this room is controllable down to -20°C and therefore capable of simulating the environmental conditions where in-flight icing can be expected.

The rotor stand was installed in the centre of the room and all cabling fed outside to the control and data acquisition system. The spray nozzles were attached to the ceiling of the cold room and, to avoid the possibility of the water lines freezing, the control solenoids and all other system hardware was mounted outside of the room with the length of water lines exposed to the cold environment kept to a minimum. The installation of the spray system and rotor thrust stand in the cold room is shown in Figure 27.

Figure 27: Spray system and rotor thrust stand installed in cold room

9 Preliminary Results

Prior to performing the full test program, a series of 'shake down' runs were performed where the system was operated over the range of environmental conditions and rotor settings shown in Table 3.

Table 3: Preliminary 'Shake down' test cases

	Test 1	Test 2	Test 3	Units
Water Flow Rate	100	50	25	cm^3/min
Atomising Air Pressure	2.5	2.5	2.5	PSI
LWC	1.9	0.8	0.3	g/m^3

MVD	120	120	120	µm
Rotor speed	4000	4000	4000	RPM
Static Temperature	-10	-10	-10	°C

Under these conditions, the rotor speed was stabilized at 4000 RPM, the water spray system initiated and, from the output of the RC Benchmark, rotor thrust, torque and power were monitored for the duration of the icing process. As a result of ice accumulation on the rotor blade, thrust was shown to reduce (along with increases in both torque and power) and it was decided to terminate the icing process once the thrust value recorded 50% of the original (non-iced) value.

Changes in thrust, torque and power compared to the values for dry air conditions, are shown in Figure 28, Figure 29 and Figure 30 respectively and show that the performance of the rotor degrades rapidly under the highest (100 cm^3/min) water flow condition. The rate of performance degradation is seen to reduce as the water flow (and therefore LWC) is reduced to 50 cm^3/min for test 2 and 25 cm^3/min for test 3. For example, with a water flow rate of 100 cm^3/min, thrust is seen to reduce by 20 N (from an initial dry air value of 47 N at spray onset) after approximately 80 seconds of exposure to the icing cloud. For the 25 cm^3/min condition, however, the time taken to reduce thrust by 15 N is approximately 400 seconds of icing exposure.

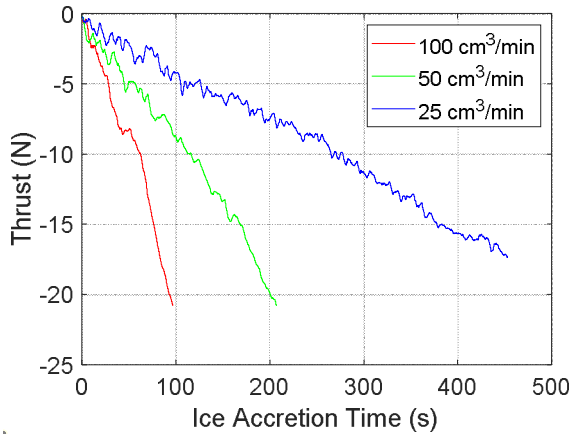

Figure 28: Rotor thrust output for icing conditions with water flow rate set to 100 cm^3/min, 50 cm^3/min and 25 cm^3/min. Change in thrust compared to dry air values of 47 N.

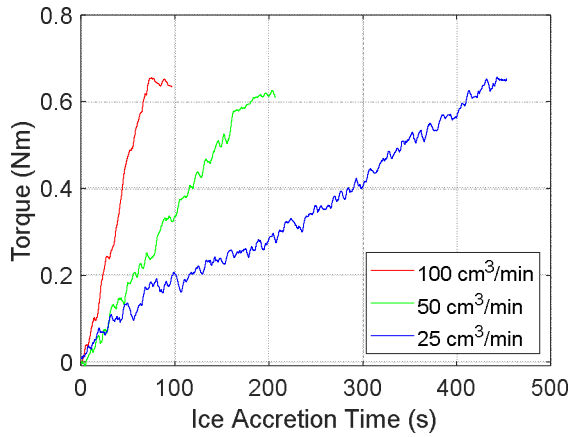

Figure 29: Rotor torque output for icing conditions with water flow rate set to 100 cm^3/min, 50 cm^3/min and 25 cm^3/min. Change in torque compared to dry air values of 1.14 Nm.

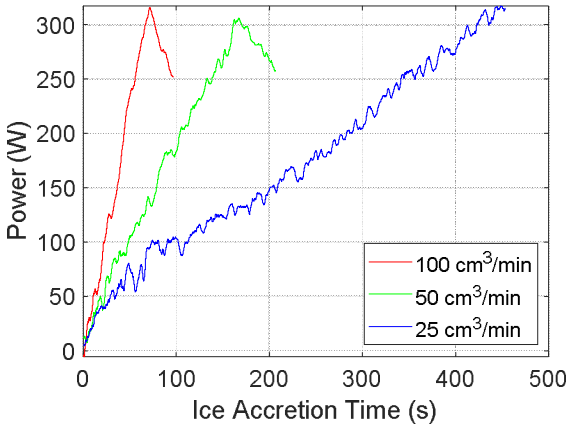

Figure 30: Rotor power output for icing conditions with water flow rate set to 100 cm^3/min, 50 cm^3/min and 25 cm^3/min. Change in power compared to dry air values of 610 W.

An image of the rotor after exposure to Test 1 icing conditions are shown in Figure 31, and indicates a layer of accreted ice at the leading edge of the blade. A further image of the rotor taken from above, shown in Figure 32, indicates that, while one half of the rotor has an even distribution of ice from the root to the tip of the blade, the opposite blade has a "clean" section where the ice has shed from the surface as a result of centrifugal forces.

Figure 31: Front view of ice accreted to leading edge of rotor following exposure to test case 1 conditions (100 cm^3/min)

Figure 32: Top view of ice accreted to leading edge of rotor following exposure to test case 1 conditions (100 cm^3/min)

10 Comparison of Small Rotor Performance in Icing

Further verification of the RPAS facility icing cloud was done by performing tests under conditions similar to those conducted in the AIWT with a 12" diameter rotor as part of Phase 2 of this research program [3]. The rotor installations in the two facilities are shown in Figure 33 and show that for the AIWT test set up, the rotor is mounted on a stand with a streamlined nacelle to shield and contain the motor and load cell assembly. For the RPAS facility, the rotor is supported with the axis aligned vertically and in this instance, due to potential aerodynamic interference from the downwash of the smaller rotor, the protective housing that surrounds the motor stand has been removed and replaced with plastic covers over the electrical components.

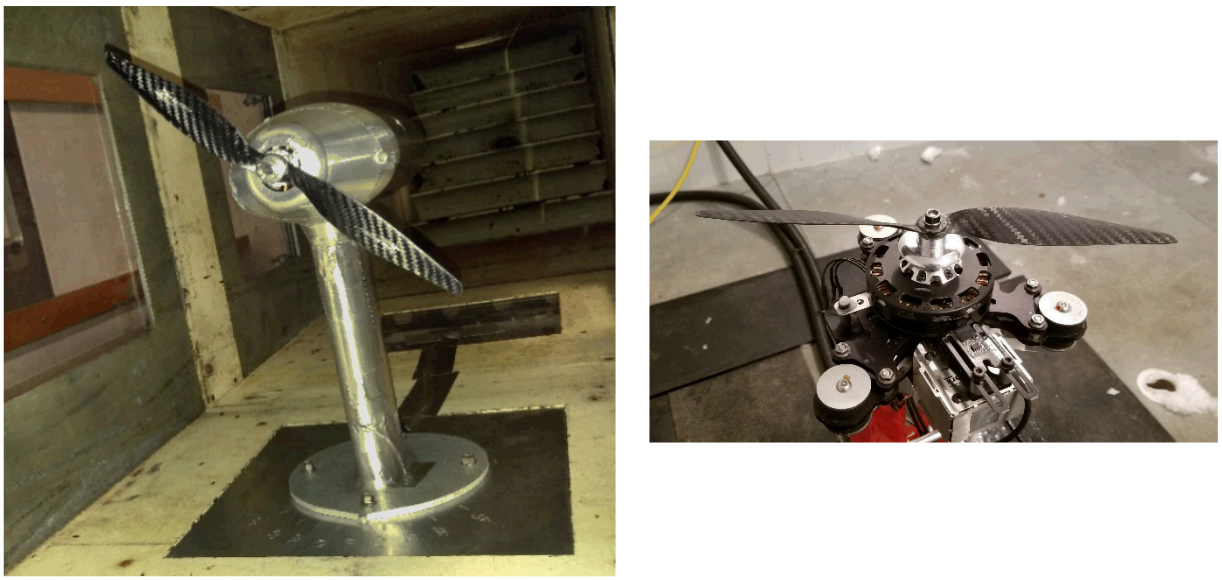

AIWT RPAS Icing Facility

Figure 33: Small rotor installation in the AIWT and RPAS icing facility

It was decided to perform two repeats tests in the RPAS facility for comparison to the data obtained in the AIWT. Firstly, the rotor performance degradation as a function of LWC was examined followed by examination of the influence of static air temperature. When studying the influence of LWC on the rotor performance, there was a key difference between the wind tunnel and RPAS facility operational conditions in that the maximum rotational speed of the motor assembly used in the RPAS assembly was 5700 RPM compared to 8000 RPM used for the AIWT installation. To compensate for this, the water flow rate for the RPAS facility tests was increased by a scale factor (i,e, 8000/5700 = 1.4) in order to maintain the same water loading on the rotor per revolution when compared to the AIWT test conditions. Further differences between the AIWT and RPAS test conditions extended to the MVD. For the AIWT test cases presented here, the MVD was set to 20 μm, however, due to the limits of the current calibration, the RPAS facility tests were performed at 60 μm. Despite the difference in MVD, this was not considered to influence the comparisons that are presented here as, during the AIWT study, rotor performance degradation was not shown to be a strong function of MVD with a close comparison in rotor output observed between the 20 μm and 60 μm test conditions [3].

The comparison of the thrust, torque and power output of the 12” diameter rotor between the AIWT and RPAS facility tests over LWCs of 0.2, 0.5 and 1.0 g/m^3 are shown in Figure 34. It is shown that for both the AIWT and RPAS facility tests, the rotor performance relative to ice exposure time is a function of LWC with, as expected, faster degradation with increasing LWC. The rate of performance degradation between the two tests is seen to differ, with the RPAS facility giving a slightly delayed retardation of thrust, torque and power when compared to the AIWT. These differences maybe be due to a number of differences between the AIWT and RPAS facility installations, e.g., the local flow profiles caused by the different motor drive assemblies, a variation between the particle spray distributions or droplet velocity (for the AIWT the wind speed, and therefore drop velocity, was held at 15m/s whereas for the RPAS facility, the drop velocity was attained via freefall from the nozzle and calculated to be less than 3 m/s for all conditions tested).

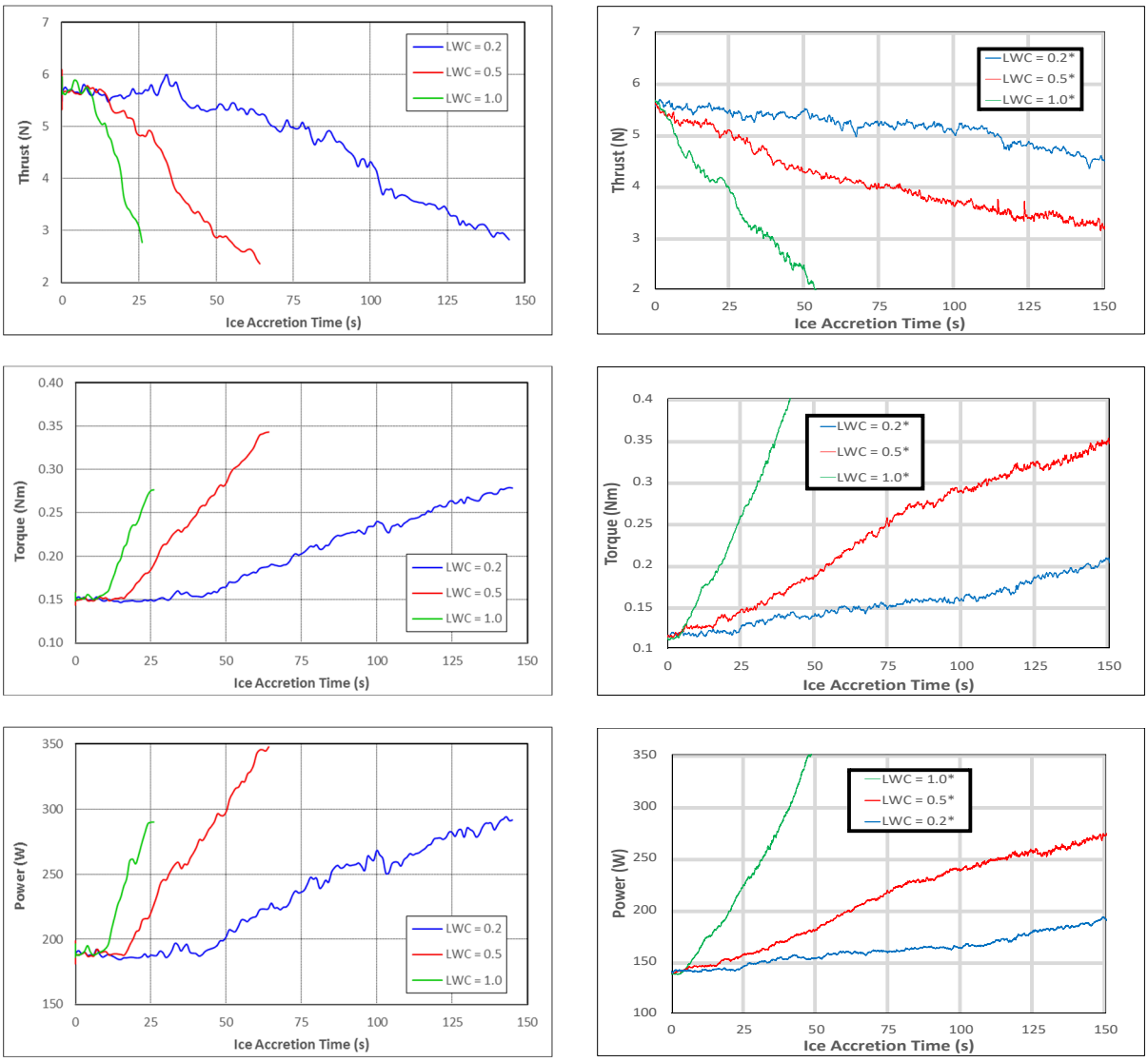

AIWT RPAS Icing Facility

**LWC scaled for water loading due to differing RPM between AIWT and RPAS icing facility operations*

Figure 34: Comparison of 12" diameter rotor performance under icing between AIWT and RPAS icing facility with variation in LWC. MVD = 60 µm and SAT = -12°C

The second comparison test between the AIWT and RPAS facility data examined the rotor performance as a function of static air temperature. For this comparison, tests conducted in the AIWT at -12°C and -5°C, LWC = 0.5 g/m^3 and MVD = 20 µm were chosen as the reference condition and, as with the LWC comparisons discussed above, for the RPAS facility these were modified to provide a scaled LWC to account for the differences in rotor RPMs and a MVD of 60 µm was used. The comparisons between the rotor performance at different static temperatures for both the AIWT and RPAS facility tests are given in Figure 35 and show that for both tests the rotor performance at-12°C degrades steadily following the onset of icing. For the -5°C condition, the output from the AIWT tests displays a 'saw tooth' appearance indicative of a cycle of accretion and shedding processes as ice builds on the rotor and eventually breaks off due to

centrifugal forces. A similar ice accretion/shedding process is observed with the RPAS facility tests, albeit slightly later compared to the AIWT output.

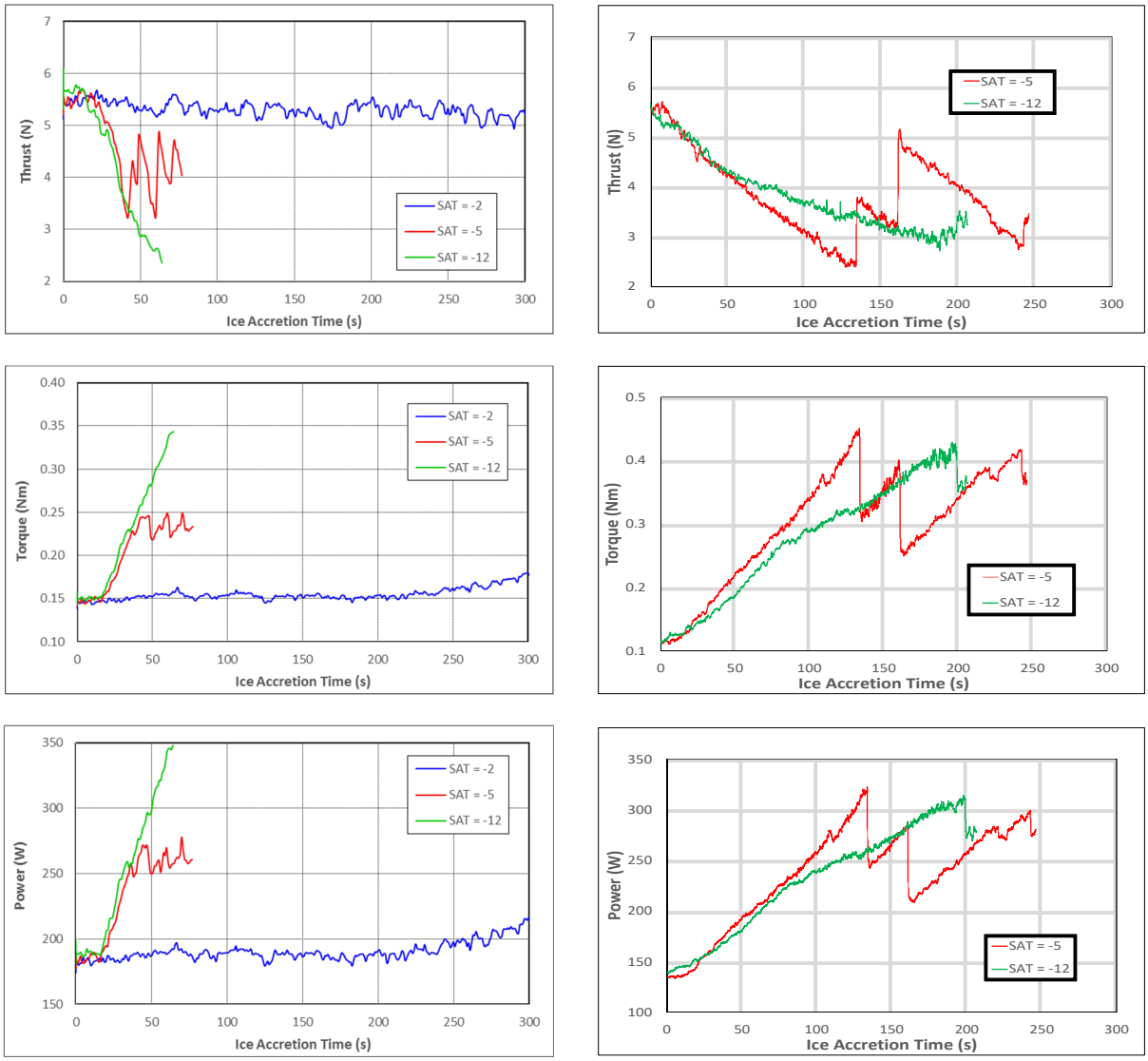

AIWT RPAS Icing Facility

Figure 35: Comparison of rotor 12" diameter performance under icing between AIWT and RPAS icing facility with variation in SAT. MVD = 60 µm and LWC = 0.5 g/m^3

Figure 36 compares the rotor ice accretion between the AIWT and RPAS facility for icing conditions at -12°C, LWC = 0.5 g/m^3 and MVD = 60 µm. While there is more ice accretion on the rotor in the RPAS facility compared to the AIWT, this is due to the extended ice exposure time (150 seconds) for the RPAS test conditions. Overall, the ice shape between the two facilities is similar, with greater ice thickness towards to tips of the rotor.

AIWT Facility

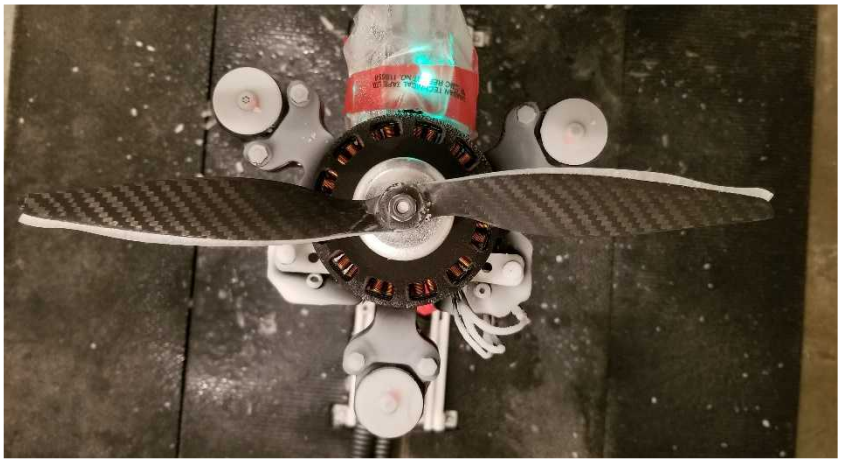

RPAS Facility

Figure 36: Ice accretion on the 12” diameter rotor in the AIWT and RPAS Facilities with LWC = 0.5 g/m^3, MVD = 60 µm and SAT = -12^{o}C

11 Conclusion

A test rig that can provide in-flight icing conditions for medium size RPAS has been developed and installed in a cold room at the Montreal Road campus of the NRC. This system has been developed to enable assessment of performance degradation of various rotor designs during encounters with in-flight icing. An extensive calibration procedure has been performed to quantify the water content and the drop size distributions of the spray system and has been compared to the in-flight conditions specified in icing regulations (e.g., 14 CFR Part 25 Appendix C and O) as well as those experienced through ground icing precipitation.

Following the calibration, preliminary testing of the rig was performed with a series of tests showing how the performance of the rotor degrades when exposed to icing conditions. In addition, a series of tests were

performed that repeat operational conditions from a previous study using a smaller (12") diameter propeller. Comparisons between the RPAS facility and the AIWT data for the smaller rotor have shown overall trends of the rotor performance under icing conditions compare well between the two facilities.

Following this calibration procedure, a series of tests on medium size propellers will be performed in the RPAS icing facility to examine the performance characteristics and degradation when exposed to various icing conditions to assist in the development of an evidence-based regulatory framework for safe UAS operations in Canadian airspace. In addition, further calibrations will be conducted to extend the operational capabilities of this facility to reflect the full in-flight icing environment of RPAS.

12 Recommendations for Future Work

This work has highlighted the calibration and test capabilities of the RPAS icing facility developed by the NRC and has demonstrated how this system can be used to assess performance of propellers and rotors in icing. It is recommended that this system be used to increase the understanding of the impact of icing on RPAS performance through further testing to evaluate the aerodynamic degradation associated with particular conditions consistent with the icing envelope identified for RPAS (e.g., drop size, rainfall (or Liquid Water Content) and ambient temperature) and thereby enable assessment of the critical operating conditions associated with in-flight icing encounters. As a result, guidance materials and/or means of compliance documentation can be developed to qualify candidate RPAS systems for flight within Canadian airspace.

Further demonstration of the NRC RPAS icing facility will provide guidance to industry in performing a critical point analysis and identifying acceptable methods that can be employed to demonstrate safe flight in representative icing conditions as part of a certification application. In addition, the work should also investigate methods by which propeller icing can be simulated via equivalent means, e.g., use of simulated ice shapes or surface roughness, and whether such an approach can be considered suitable when demonstrating means of compliance.

13 Acknowledgements

The present work was funded by Transport Canada, RPAS Task Force Engineering.

The Author would like to thank Dan Gendreau for his efforts in the development of the spray rig and rotor test stand as well as Gislain Chevrette for sharing his extensive knowledge on spray system design and implementation.

14 References

1. Civil Aviation Authority (New Zealand), "Aircraft Icing Handbook", 2000
2. Benmeddour, A., "Investigation of Tolerance for Icing of Small UAV Rotors/Propellers – Phase 1", LTR-AL-2019-0024, Aerodynamics Laboratory, NRC- Aerospace
3. Benmeddour, A., "Investigation of Tolerance for Icing of Small UAV Rotors/Propellers – Phase 2", LTR-AL-2019-0053, Aerodynamics Laboratory, NRC- Aerospace
4. Federal Aviation Administration, "Part 25: Airworthiness Standard: Transport Category Airplanes, Appendix C. Title 14: Aeronautics and Space, U.S., Code of Federal Regulations", 1999.
5. National Transportation Safety Board, "In-Flight Icing Encounter and Loss of Control Simmons Airlines, d. b. a. American Eagle Flight 4184 Avions de Transport Regional (ATR) Model 72-212, N401AM, Roselawn, Indiana", NTSB/AAR-96/01, 1994.
6. Federal Aviation Administration, "Part 25: Airworthiness Standard: Transport Category Airplanes, Appendix O. Title 14: Aeronautics and Space, U.S., Code of Federal Regulations", 2015.

7. Cober, S.G., Bernstein, B, Jeck, R., Hill, E., Isaac, G., Riley, J. and Shah, A., “Data and Analysis for the development of an Engineering Standard for Supercooled Large Drop Conditions”, U.S. Department of Transportation Final Report, DOT/FAA/AR-09/10, 2009.
8. Cober, S.G. and Isaac, G.A., “Characterization of Aircraft Icing Environments with Supercooled Large Drops for Application to Commercial Aircraft Certification”, Journal of Applied Meteorology and Climatology, Volume 51, 265-284, 2012.
9. R.J. Schulz, “Second Report for Research and Modelling of Water Particles in Adverse Weather Simulation Facilities”, AEDC TASK report 97-03
10. R.J. Schulz, “A Model for Predicting Mixed-Phase Flow in Ground Test Facilities”, 37th AIAA Aerospace Sciences Meeting and Exhibit, AIAA 99-0308, January 1999, Reno, NV.